NUMERICAL APPROXIMATION OF KNUDSEN LAYER FOR THE EULER-POISSON SYSTEM

FRÉDERIQUE CHARLES[1], NICOLAS VAUCHELET[1], CHRISTOPHE BESSE[2, 3], THIERRY GOUDON[2,3], INGRID LACROIX–VIOLET[2,3], JEAN-PAUL DUDON[4] AND LAURENT NAVORET[5]

Abstract. In this work, we consider the computation of the boundary conditions for the linearized Euler–Poisson derived from the BGK kinetic model in the small mean free path regime. Boundary layers are generated from the fact that the incoming kinetic flux might be far from the thermodynamical equilibrium. In [2], the authors propose a method to compute numerically the boundary conditions in the hydrodynamic limit relying on an analysis of the boundary layers. In this paper, we will extend these techniques in the case of the coupled Euler-Poisson system.

Résumé. Dans ce travail, nous nous intéressons à l'évaluation numérique de conditions aux limites pour le système d'Euler–Poisson linéarisé obtenu à partir du modèle cinétique BGK dans le régime de petit libre parcours moyen. Des couches limites peuvent apparaître en raison du fait que les flux cinétiques entrants peuvent différer de l'équilibre thermodynamique. La réference [2] introduit une méthode de calcul numérique des conditions aux limites dans un tel régime hydrodynamique basée sur l'analyse des couches limites. Ici, nous étendons ces techniques au cas du système couplé d'Euler–Poisson.

1. INTRODUCTION

At a kinetic level, a statistical description of the dynamics of a plasma subject to an electric field $E(t,x)$ can be obtained thanks to the Boltzmann equation governing the evolution of the particles distribution function $F(t,x,v)$. In the one dimensional framework, this equation reads:

$$\partial_t F + v\partial_x F + qE\partial_v F = \frac{1}{\tau}Q(F), \tag{1}$$

where $q \in \{-1, 1\}$ correspond to the sign of the charge of particles. Here the time variable $t \geq 0$, the position variable x belongs to $(-\omega, \omega) \subset \mathbb{R}$ and the velocity $v \in \mathbb{R}$. The parameter τ is the Knudsen number; it is related to the mean free path and is assumed to be small. In this work, we choose for the collision operator Q the BGK collision operator:

$$Q(F) = M_{(\rho,u,\theta)} - F,$$

where the Maxwellian

$$M_{(\rho,u,\theta)}(v) = \frac{\rho}{\sqrt{2\pi\theta}}\exp\left(-\frac{|v-u|^2}{2\theta}\right), \tag{2}$$

---

[1] Laboratoire Jacques-Louis Lions - UMR 7598 CNRS & Université Pierre et Marie Curie, Paris VI
[2] Project Team SIMPAF, INRIA Lille Nord Europe
[3] Labo Paul Painlevé UMR 8524, CNRS & USTLille
[4] Thales Alenia Space, Cannes
[5] Institut Mathématique de Toulouse CNRS & Université Paul Sabatier, Toulouse

and the macroscopic quantities (ρ, u, θ) are defined by

$$\text{density}: \qquad \rho(t,x) = \int_{\mathbb{R}} F(t,x,v)\, dv,$$

$$\text{velocity}: \qquad \rho u = \int_{\mathbb{R}} v F(t,x,v)\, dv,$$

$$\text{temperature}: \qquad \rho u^2 + \rho \theta = \int_{\mathbb{R}} |v|^2 F(t,x,v)\, dv.$$

In this paper we restrict to consider a single specie of charged particles, the particles of the opposite charge being a given background with a fixed and constant density. The electric field $E = -\partial_x V$ is self-consistently defined through the Poisson equation satisfied by the potential V:

$$-\partial_{xx} V = q(\rho - 1). \tag{3}$$

We recall that $(1, v, |v|^2)$ are collision invariants:

$$\int_{\mathbb{R}} \begin{pmatrix} 1 \\ v \\ |v|^2 \end{pmatrix} Q(F)\, dv = 0. \tag{4}$$

It is well-known that when $\tau \to 0$, the distribution function F converges to a Maxwellian, whose macroscopic parameters ρ, u and θ solves the Euler system. The question raised by this work is the determination of the boundary conditions on this Euler system corresponding to the ones imposed on the kinetic system. Here system (1)–(3) is completed with the following boundary conditions:

$$\gamma^{inc} F(t, -\omega, v) = \mathcal{R}(\gamma^{out} F(t, -\omega, \cdot))(v) + \Phi^{data,L}(t, v), \qquad \text{for } v > 0, \tag{5}$$

$$\gamma^{inc} F(t, \omega, v) = \mathcal{R}(\gamma^{out} F(t, \omega, \cdot))(v) + \Phi^{data,R}(t, v), \qquad \text{for } v < 0, \tag{6}$$

where $\Phi^{data,R}$ and $\Phi^{data,L}$ are given functions, and $\mathcal{R}$ is a reflection operator. For instance assuming $\mathcal{R} = 0$ and $\Phi^{data} = 0$ corresponds to a fully absorbing boundary. We consider here two types of reflection operator: the specular reflection operator given by

$$\mathcal{R}(F)(t, x, v) = \alpha F(t, x, -v), \tag{7}$$

where the parameter $\alpha \in [0, 1]$ represents the fraction of reflected particles, and the reflection operator of the Maxwell diffuse law given by

$$\mathcal{R}(F)(t, -\omega, v) = \alpha \frac{M_w(v)}{Z_w} \int_{v' < 0} |v'| F(t, -\omega, v')\, dv', \qquad \text{for } v > 0, \tag{8}$$

where

$$M_w(v) = \frac{\rho_w}{\sqrt{2\pi\theta_w}} e^{-|v|^2/(2\theta_w)}, \quad Z_w = \int_{v > 0} v M_w(v)\, dv,$$

with θ_w the temperature of the wall (see e.g. [15]). Obviously, dealing with the right hand boundary, $+\omega$ replaces $-\omega$ and incoming particles have negative velocities $v < 0$, we change the sign of v' in (8) accordingly. The problem is also completed with an initial condition

$$F(0, x, v) = F^{init}(x, v).$$

For the Poisson equation, we impose Dirichlet boundary conditions

$$V(t, -\omega) = V^L, \qquad V(t, \omega) = V^R.$$

This framework might appear quite crude in comparison to the complex boundary conditions that are used in plasma physics, where the boundary potential depends on the particles fluxes, see e. g. [6–8, 17, 20, 23]

and the references therein. We restrict to this simple situation in order to bring out clearly the ideas and it already make several difficulties appear; we shall go back to a more ambitious model elsewhere.

As the mean free path goes to 0, the kinetic model can be approached by a system of conservation laws for which the number of boundary conditions that should be fixed depends on the solution itself (see e.g. [9]). In fact the boundary conditions for the hyperbolic system depend on the number of incoming characteristics at the boundary. The aim of this work is to present numerical methods to compute the boundary fluxes for the hydrodynamic model, and to compare the results with simulations of the kinetic equation (1).

The paper is organized as follows. In the next Section, we study the simplest case where we linearize the Boltzmann–BGK equation around a Maxwellian steady state. We first introduce some notations and recall the theoretical results needed. Then we present some numerical simulations. In Section 3, we are concerned with the coupling with the Poisson equation. We consider both the linearized problem and the non-linear case.

2. Analysis for the linearized Euler system

In this section, we are interested in the numerical approximation of the boundary layer for the linearized Euler system in the case $E = 0$, i.e. there is no coupling with the Poisson equation.

2.1. Analysis of the boundary layer

We briefly recall here the theorical results developped in [9] (see also [13]). Let us assume that $\rho_* > 0$, $\theta_* > 0$ and $u_* \in \mathbb{R}$ are given. We verify easily that $M_* := M_{(\rho_*, u_*, \theta_*)}$ is a stationary solution of (1) with $E = 0$. Linearizing around the equilibrium M_* in the form $F = M_*(1 + f)$, (1) leads to the linearized equation for f:

$$\partial_t f + v \partial_x f = \frac{1}{\tau} L_*(f), \tag{9}$$

where L_* is the linearized BGK operator. More precisely, for $f \in L^2(M_* \, dv)$ we have $L_*(f) = \Pi f - f$, with Π the orthogonal projection of $L^2(M_* \, dv)$ to the finite dimensional set spanned by the collisional invariant $\{1, v, |v|^2\}$ (see [2]):

$$\Pi f = \frac{\widetilde{\rho}}{\rho_*} + \frac{v - u_*}{\theta_*} \widetilde{u} + \left(\frac{|v - u_*|^2}{\theta_*} - 1 \right) \frac{\widetilde{\theta}}{2\theta_*},$$

where $(\widetilde{\rho}, \widetilde{u}, \widetilde{\theta})$ are such that

$$\begin{pmatrix} \widetilde{\rho} \\ \widetilde{\rho} u_* + \rho_* \widetilde{u} \\ \widetilde{\rho}(u_*^2 + \theta_*) + 2\rho_* u_* \widetilde{u} + \rho_* \widetilde{\theta} \end{pmatrix} = \int_{\mathbb{R}} \begin{pmatrix} 1 \\ v \\ |v|^2 \end{pmatrix} f M_* \, dv.$$

We can verify that the following properties[1] hold:

- L_* is self-adjoint for the inner product of $L^2(M_* \, dv)$,
- $\mathrm{Ker}(L_*) = \mathrm{Span} \{1, v, |v|^2\}$,
- $\mathrm{Ran}(L_*) = (\mathrm{Ker}(L_*))^{\perp}$ for the inner product of $L^2(M_* \, dv)$,
- we have the dissipation property

$$\int_{\mathbb{R}} L_* f f M_* \, dv \leq 0.$$

Equation (9) is completed with the boundary conditions deduced from (5)–(6)

$$\gamma^{inc}(M_* f)(t, -\omega, v) = \mathcal{R}(\gamma^{out}(M_* f)(t, -\omega, \cdot))(v) + \phi^{data,L}(t, v), \quad \text{for } v > 0, \tag{10}$$

$$\gamma^{inc}(M_* f)(t, \omega, v) = \mathcal{R}(\gamma^{out}(M_* f)(t, \omega, \cdot))(v) + \phi^{data,R}(t, v), \quad \text{for } v < 0, \tag{11}$$

---

[1]These properties obviously hold for the linearized BGK operator because it reduces to a mere projection; but it is important to bring out the crucial analytical properties required to extend the discussion to more intricate operators

where for instance in the case $v > 0$, we have

$$\phi^{data,L} = \Phi^{data,L} - M_* + \mathcal{R}(M_*),$$

and with the initial data

$$f(0, x, v) = f^{init}(x, v).$$

Formally, when $\tau \to 0$ the function f belongs to $\mathrm{Ker}(L_*)$ and can be therefore described by an infinitesimal Maxwellian:

$$m_{(\widetilde{\rho}, \widetilde{u}, \widetilde{\theta})(t,x)}(v) = \frac{\widetilde{\rho}}{\rho_*} + \frac{v - u_*}{\theta_*}\widetilde{u} + \left(\frac{|v - u_*|^2}{\theta_*} - 1\right)\frac{\widetilde{\theta}}{2\theta_*}. \tag{12}$$

From (9) and the definition of $\mathrm{Ker}(L_*)$ we deduce the moment system:

$$\partial_t \int_{\mathbb{R}} \begin{pmatrix} 1 \\ v \\ |v|^2 \end{pmatrix} f M_* \, dv + \partial_x \int_{\mathbb{R}} v \begin{pmatrix} 1 \\ v \\ |v|^2 \end{pmatrix} f M_* \, dv = 0.$$

Substituting f by the infinitesimal Maxwellian $m_{(\widetilde{\rho}, \widetilde{u}, \widetilde{\theta})}$ leads to the linearized Euler system:

$$\partial_t \begin{pmatrix} \widetilde{\rho} \\ \widetilde{u} \\ \widetilde{\theta} \end{pmatrix} + \begin{pmatrix} u_* & \rho_* & 0 \\ \frac{\theta_*}{\rho_*} & u_* & 1 \\ 0 & 2\theta_* & u_* \end{pmatrix} \partial_x \begin{pmatrix} \widetilde{\rho} \\ \widetilde{u} \\ \widetilde{\theta} \end{pmatrix} = 0. \tag{13}$$

The system (13) writes in matrix form

$$\partial_t \widetilde{U} + A \partial_x \widetilde{U} = 0, \tag{14}$$

with

$$A = \begin{pmatrix} u_* & \rho_* & 0 \\ \frac{\theta_*}{\rho_*} & u_* & 1 \\ 0 & 2\theta_* & u_* \end{pmatrix}.$$

This system is obviously hyperbolic: the spectrum of the matrix A is $\{u_* - \sqrt{3\theta_*}, u_*, u_* + \sqrt{3\theta_*}\}$. Therefore, the number of boundary conditions that should be fixed at the left (resp. right) boundary depends on the number of positive (resp. negative) eigenvalues. Moreover, we can define the following quadratic form

$$\mathbf{Q} : \widetilde{U} = (\widetilde{\rho}, \widetilde{u}, \widetilde{\theta}) \mapsto \int_{\mathbb{R}} v |m_{(\widetilde{\rho}, \widetilde{u}, \widetilde{\theta})}|^2 \, M_* \, dv. \tag{15}$$

Following [2, 9], we can split the set of infinitesimal Maxwellians according to the sign of the quadratic form $\mathbf{Q}$:

$$\mathrm{Ker}(L_*) = \Lambda^+ \oplus \Lambda^- \oplus \Lambda^0,$$

where $\Lambda^{\pm}$ corresponds to the eigenspaces associated to the positive (resp. negative) eigenvalues of A, and Λ^0 is the eigenspace associated to 0 when it belong to the spectrum of A. We shall denote $I^{\pm} = \dim(\Lambda^{\pm})$ the number of positive (resp. negative) eigenvalues of A.

Then, considering the left hand boundary $x = -\omega$, it is possible to split $m_{(\widetilde{\rho}, \widetilde{u}, \widetilde{\theta})}$ into $m_- \in \Lambda^-$ (which corresponds to the "outgoing part") and $m_+ \in \Lambda^+ \oplus \Lambda^0$ (which corresponds to the "incoming part" at the boundary $x = -\omega$) :

$$m_{(\widetilde{\rho}, \widetilde{u}, \widetilde{\theta})} = m_- + m_+. \tag{16}$$

Dealing with the right hand boundary $x = +\omega$, the role of Λ^+ and Λ^- is inverted. At each boundary the outgoing part is given by the flow, whereas the incoming part has to be imposed as a boundary condition to complete the Euler system.

The incoming flux at the boundaries are determined thanks to a boundary layer analysis. Let us consider the following half space problem

$$\begin{cases} v \partial_z G = L_* G, & z > 0, \ v \in \mathbb{R} \\ G(0, v) = \Upsilon^{data}, & v > 0 \end{cases} \tag{17}$$

where Υ^{data} has to be suitably defined. We recall the following statement (see [9]):

Theorem 1. *There exists a linear mapping (that is usually called the generalized Chandrasekhar functional)*

$$\mathcal{C}_* : \quad L^2(\mathbb{R}, (1 + |v|)M_*(v)\, dv) \quad \rightarrow \quad \Lambda^+ \oplus \Lambda^0$$
$$\Upsilon^{data} \quad\quad\quad\quad\quad \mapsto \quad m_\infty,$$

where m_∞ is the limit as $z \to \infty$ of the unique solution G of (17). Moreover, $G \in L^\infty(0, \infty; L^2(\mathbb{R}, M_*(v)\, dv))$.

Let us assume that f expands as follows

$$f = m_{(\widetilde{\rho}, \widetilde{u}, \widetilde{\theta})} + G^L\left(t, \frac{x + \omega}{\tau}, v\right) + G^R\left(t, \frac{\omega - x}{\tau}, v\right) + o(\tau),$$

where G^L and G^R stand for boundary layers and are defined as follows :

- $G^L(t, z, v) = G(t, z, v)$ with G the solution of (17) with incoming data

$$\Upsilon^{data}(t, v) = \gamma^{inc} f(t, -\omega, v) - m_{(\widetilde{\rho}, \widetilde{u}, \widetilde{\theta})}(t, -\omega, v), \tag{18}$$

and imposing that

$$\lim_{z \to +\infty} G(z, v) = 0, \tag{19}$$

- $G^R(t, z, v) = G(t, z, -v)$ with G the solution of (17) with incoming data

$$\Upsilon^{data}(t, v) = \gamma^{inc} f(t, \omega, -v) - m_{(\widetilde{\rho}, \widetilde{u}, \widetilde{\theta})}(t, \omega, -v). \tag{20}$$

and condition (19).

Condition (19) expresses that the boundary layer is expected to vanish far from the boundary. Using the decomposition on $\mathrm{Ker}(L_*)$ in (16), it implies that the unknown m_+ satisfies

$$\mathcal{C}_*(\gamma^{inc} f(t, \omega, \cdot) - m_-(t, \omega, \cdot)) = \mathcal{C}_*(m_+(t, \omega, \cdot)), \qquad \mathcal{C}_*(\gamma^{inc} f(t, -\omega, \cdot) - m_-(t, -\omega, \cdot)) = \mathcal{C}_*(m_+(t, -\omega, \cdot)). \tag{21}$$

The question we address is concerned with the numerical approximation of the outgoing state m^+, which arises in the definition of the boundary fluxes.

2.2. Numerical resolution of the linearized Euler system

2.2.1. *Numerical method*

The matrix A of the system (13) can be diagonalized under the form

$$A = \begin{pmatrix} u_* & \rho_* & 0 \\ \frac{\theta_*}{\rho_*} & u_* & 1 \\ 0 & 2\theta_* & u_* \end{pmatrix} = P \begin{pmatrix} u_* & 0 & 0 \\ 0 & u_* + \sqrt{3\theta_*} & 0 \\ 0 & 0 & u_* - \sqrt{3\theta_*} \end{pmatrix} P^{-1},$$

with

$$P = \frac{1}{2\sqrt{\theta_*}} \begin{pmatrix} 2\sqrt{\theta_*}\rho_* & \sqrt{3}\rho_* & -\sqrt{3}\rho_* \\ 0 & 3\sqrt{\theta_*} & 3\sqrt{\theta_*} \\ -2\sqrt{\theta_*}\theta_* & 2\theta_*\sqrt{3} & -2\theta_*\sqrt{3} \end{pmatrix}, \qquad P^{-1} = \frac{1}{3\rho_*\sqrt{3\theta_*}} \begin{pmatrix} 2\sqrt{3\theta_*} & 0 & -\rho_*\sqrt{3}/\sqrt{\theta_*} \\ \theta_* & \rho_*\sqrt{3\theta_*} & \rho_* \\ -\theta_* & \rho_*\sqrt{3\theta_*} & -\rho_* \end{pmatrix}.$$

We set

$$\begin{pmatrix} \widetilde{\rho}_{diag} \\ \widetilde{u}_{diag} \\ \widetilde{\theta}_{diag} \end{pmatrix} = P^{-1} \begin{pmatrix} \widetilde{\rho} \\ \widetilde{u} \\ \widetilde{\theta} \end{pmatrix}$$

the variables in the new basis defined by the transition matrix P, and we obtain three independant equations on $\tilde{\rho}_{diag}$, $\tilde{u}_{diag}$, $\tilde{\theta}_{diag}$:

$$\begin{cases} \partial_t \tilde{\rho}_{diag} + u_* \partial_x \tilde{\rho}_{diag} = 0, & \text{(a)} \\ \partial_t \tilde{u}_{diag} + (u_* + \sqrt{3\theta_*}) \partial_x \tilde{u}_{diag} = 0, & \text{(b)} \\ \partial_t \tilde{\theta}_{diag} + (u_* - \sqrt{3\theta_*}) \partial_x \tilde{\theta}_{diag} = 0. & \text{(c)} \end{cases} \tag{22}$$

Equations (22) should be completed with boundary conditions, which depend on the sign of u_*, $u_* + \sqrt{3\theta_*}$ and $u_* - \sqrt{3\theta_*}$. More precisely, we denote $U_{bd,l} = (\rho_{bd,l}, u_{bd,l}, \theta_{bd,l})$ and $U_{bd,r} = (\rho_{bd,r}, u_{bd,r}, \theta_{bd,r})$ the macroscopic quantities which have to be defined at the boundaries $x = -\omega$ and $x = \omega$ respectively, and we set

$$\mathcal{U}_{bd,l} = \begin{pmatrix} \mathcal{U}_{bd,l}^1 \\ \mathcal{U}_{bd,l}^2 \\ \mathcal{U}_{bd,l}^3 \end{pmatrix} = P^{-1} U_{bd,l}, \quad \mathcal{U}_{bd,r} = \begin{pmatrix} \mathcal{U}_{bd,r}^1 \\ \mathcal{U}_{bd,r}^2 \\ \mathcal{U}_{bd,r}^3 \end{pmatrix} = P^{-1} U_{bd,r}.$$

Boundary conditions of equations (22) are :

$$\begin{array}{llll} \tilde{\rho}_{diag}(-\omega) = \mathcal{U}_{bd,l}^1 \text{ if } u_* > 0 & \text{or} & \tilde{\rho}_{diag}(\omega) = \mathcal{U}_{bd,r}^1 \text{ if } u_* < 0, & \text{(a)} \\ \tilde{u}_{diag}(-\omega) = \mathcal{U}_{bd,l}^2 \text{ if } u_* + \sqrt{3\theta_*} > 0 & \text{or} & \tilde{u}_{diag}(\omega) = \mathcal{U}_{bd,r}^2 \text{ if } u_* + \sqrt{3\theta_*} < 0, & \text{(b)} \\ \tilde{\theta}_{diag}(-\omega) = \mathcal{U}_{bd,l}^3 \text{ if } u_* - \sqrt{3\theta_*} > 0 & \text{or} & \tilde{\theta}_{diag}(\omega) = \mathcal{U}_{bd,r}^3 \text{ if } u_* - \sqrt{3\theta_*} < 0. & \text{(c)} \end{array} \tag{23}$$

We then introduce a regular subdivision $\{x_0, \ldots, x_{I+1}\}$ of the domain $[-\omega, \omega]$, with $x_i = -\omega + i\Delta x$ and $\Delta x = 2\omega/(I+1)$, and a time discretisation Δt. Equations (22) are solved numerically thanks to an upwind scheme. We obtain for instance, thanks to equation (22)-(a) and boundary condition (23)-(a), the following approximations $\tilde{\rho}_{diag,i}^n$ of $\tilde{\rho}_{diag}(n\Delta t, x_i)$:

$$\begin{cases} \tilde{\rho}_{diag,0}^{n+1} = \mathcal{U}_{bd,l}^{1,n+1}, \\ \tilde{\rho}_{diag,1}^{n+1} = \tilde{\rho}_{diag,1}^n - u_* \dfrac{\Delta t}{\Delta x}\left(\tilde{\rho}_{diag,1}^n - \mathcal{U}_{bd,l}^{1,n}\right), & \text{if } u_* > 0, \\ \tilde{\rho}_{diag,i}^{n+1} = \tilde{\rho}_{diag,i}^n - u_* \dfrac{\Delta t}{\Delta x}(\tilde{\rho}_{diag,i}^n - \tilde{\rho}_{diag,i-1}^n) & \text{for } i \in \{2, I+1\}, \end{cases}$$

and

$$\begin{cases} \tilde{\rho}_{diag,i}^{n+1} = \tilde{\rho}_{diag,i}^n - u_* \dfrac{\Delta t}{\Delta x}(\tilde{\rho}_{diag,i+1}^n - \tilde{\rho}_{diag,i}^n) & \text{for } i \in \{0, I-1\}, \\ \tilde{\rho}_{diag,I}^{n+1} = \tilde{\rho}_{diag,I}^n - u_* \dfrac{\Delta t}{\Delta x}\left(\mathcal{U}_{bd,r}^{1,n} - \tilde{\rho}_{diag,I}^n\right), & \text{if } u_* < 0, \\ \tilde{\rho}_{diag,I+1}^{n+1} = \mathcal{U}_{bd,r}^{1,n+1}, \end{cases}$$

where $\mathcal{U}_{bd,l}^{1,n} = \mathcal{U}_{bd,l}^1(n\Delta t)$ and $\mathcal{U}_{bd,r}^{1,n} = \mathcal{U}_{bd,r}^1(n\Delta t)$. These values are computed by solving (21). The method to solve these equations is explained in the next subsection. We denote in the sequel

$$\tilde{U}_i^n = \begin{pmatrix} \tilde{\rho}_i^n \\ \tilde{u}_i^n \\ \tilde{\theta}_i^n \end{pmatrix} = P \begin{pmatrix} \tilde{\rho}_{diag,i}^n \\ \tilde{u}_{diag,i}^n \\ \tilde{\theta}_{diag,i}^n \end{pmatrix}. \tag{24}$$

2.2.2. *Treatment of the boundary conditions*

We explain in this section the method presented in [2] to compute, at each time step, the hydrodynamic boundary conditions $U_{bd,l}^n$ and $U_{bd,r}^n$ from the knowledge of the hydrodynamic quantity $\tilde{U}_i^n$ near the boundaries $x = \pm\omega$ and the knowledge of $\phi^{data,L}$, $\phi^{data,R}$ and $\mathcal{R}$ in (10).

We focus here the discussion on the boundary $x = -\omega$ (the treatment of the boundary $x = \omega$ is similar). We introduce, at each time $t^n = n\Delta t$, the infinitesimal Maxwellian

$$m_{bd,l}^n(v) = \frac{\rho_{bd,l}^n}{\rho_*} + u_{bd,l}^n \frac{v - u_*}{\theta_*} + \frac{\theta_{bd,l}^n}{2\theta_*}\left(\frac{(v - u_*)^2}{\theta_*} - 1\right)$$

and we associate to $m_{bd,l}^n$ its decomposition on $Ker(L_*)$ as in (16) :

$$m_{bd,l}^n = m_+^n + m_-^n. \tag{25}$$

The outgoing part $m_-^n \in \Lambda^-$ is given by the projection of $\tilde{U}_0^n$ on Λ^- :

$$m_-^n(v) = \sum_{k \in I_-} \alpha_k^n \chi_k(v), \quad \alpha_k^n = \frac{\int_{\mathbb{R}} v\, m_{\tilde{U}_0^n} \chi_k(v)\, M_{\rho_*,u_*,\theta_*}(v) dv}{\int_{\mathbb{R}} v\, |\chi_k(v)|^2\, M_{\rho_*,u_*,\theta_*}(v) dv},$$

where $m_{\tilde{U}_0^n}$ is defined in (12). We denote (χ_0, χ_1, χ_2) an orthogonal basis of $Ker(L_*)$ which is here defined by (see [2])

$$\chi_0(v) = \frac{1}{\sqrt{6}}\left(\frac{|v - u_*|^2}{\theta_*} - 3\right),$$

$$\chi_1(v) = \frac{1}{\sqrt{6}}\left(\sqrt{3}\frac{v - u_*}{\sqrt{\theta_*}} + \frac{|v - u_*|^2}{\theta_*}\right),$$

$$\chi_2(v) = \frac{1}{\sqrt{6}}\left(\sqrt{3}\frac{v - u_*}{\sqrt{\theta_*}} - \frac{|v - u_*|^2}{\theta_*}\right),$$

and

$$I^+ = \left\{k \in \{0,1,2\}, \chi_k \in \Lambda^+\right\}, \quad I^- = \left\{k \in \{0,1,2\}, \chi_k \in \Lambda^-\right\}, \quad I^0 = \left\{k \in \{0,1,2\}, \chi_k \in \Lambda^0\right\}.$$

Moreover,

$$\mathbf{Q}(\chi_0) = \rho_* u_*, \quad \mathbf{Q}(\chi_1) = \rho_*(u_* + \sqrt{3\theta_*}), \quad \mathbf{Q}(\chi_2) = \rho_*(u_* - \sqrt{3\theta_*}),$$

where $\mathbf{Q}$ is the quadratic form defined in (15). Consequently, the sign of the eigenvalues $u_* - \sqrt{3\theta_*}$, u_*, $u_* + \sqrt{3\theta_*}$ allows us to know I^- and therefore to compute m_-^n.

Then we need to compute m_+^n. We first notice that integrating the half space problem (17) over the velocity variable gives

$$\frac{d}{dz} \int_{\mathbb{R}} v \begin{pmatrix} 1 \\ v \\ |v|^2 \end{pmatrix} G^L(z,v) M_*(v) dv = 0,$$

and then

$$\int_{\mathbb{R}} v \begin{pmatrix} 1 \\ v \\ |v|^2 \end{pmatrix} G^L(0,v) M_*(v) dv = \int_{\mathbb{R}} v \begin{pmatrix} 1 \\ v \\ |v|^2 \end{pmatrix} G^L(\infty,v) M_*(v) dv = 0. \tag{26}$$

Moreover, we make an approximation proposed by Maxwell in [19] (see also [1, 18]) : we assume that the outgoing distribution at the boundary $\gamma^{out} G_L(0, \cdot)$ coincides with the distribution at infinity, that is to say

$$\gamma^{out} G(0,v) = \lim_{z \to +\infty} G(z,v) = 0, \qquad v > 0. \tag{27}$$

Then, using (26), (20) and (27), we obtain

$$\int_{v>0} v \begin{pmatrix} 1 \\ v \\ |v|^2 \end{pmatrix} \left[\gamma^{inc}(f) - m_{bd,l}^n\right] M_* dv = 0. \tag{28}$$

7

Finally, thanks to (10) and (25), we get

$$\int_{v>0} v \begin{pmatrix} 1 \\ v \\ |v|^2 \end{pmatrix} \left[\phi^{data,L}(t^n, v) + \mathcal{R}(M_* m_-^n)(v) - m_-^n(v) M_*(v) \right] dv$$

$$= \int_{v>0} v \begin{pmatrix} 1 \\ v \\ |v|^2 \end{pmatrix} \left(m_+^n(v) M_*(v) - \mathcal{R}(M_* m_+^n)(v) \right) dv. \tag{29}$$

Relation (29) allows us to compute m_+^n. We notice that we have three equations for m_+^n to be satisfied whereas $\dim(\Lambda^+ \oplus \Lambda^0) \in \{0, 1, 2, 3\}$. In the case $u_* = 0$ i.e. when the signature of the quadratic form $\mathbf{Q}$ is $(1, 1)$, we use the fact that we have the additional conservation law (see [2, 14])

$$\frac{d}{dz} \int_{\mathbb{R}} v^2 \chi_0(v) G(z, v) M_{(\rho_*, 0, \theta_*)}(v) \, dv = 0.$$

A method to solve this overdeterminated problem is to pick the number of equations needed in (29) (see [14]). Here we will follow instead the method in [2] where the determination of m_+^n relies on the resolution of a least squares problem under constraints. We refer to [2] for further details.

2.3. **Numerical comparisons**

The equation (9) is solved thanks to a splitting scheme : we solve successively the free transport equation $\partial_t f + v \partial_x f = 0$ (with upwind scheme) and the collision part $\partial_t f = \frac{1}{\tau} L_*(f)$. We notice that this last equation can be solved exactly since by conservation properties, a solution f of this equation satisfies $\frac{d}{dt} \int_{\mathbb{R}} (1, v, v^2) f(v) \, dv = 0$, and therefore Πf is not modified during this step and can be considered as a given source term. We refer to [2] for further details. In the simulation presented below, we take $\Delta v = 5 \cdot 10^{-4}$ and $\tau = 10^{-3}$, and for both hydrodynamic and kinetic simulation $\omega = 0.5$ and $\Delta x = 1/500$ (in convenient units). The final time is $t_f = 0.1$ and the time step Δt is determined by the CFL condition. We then compare the numerical solution of the linearized Boltzmann equation (9) with the numerical solution of linearized Euler system (14).

On Figure 1, we consider the equilibrium state given by

$$(\rho_*, u_*, \theta_*) = (1, -0.1, 1),$$

with specular reflection at boundaries (operator $\mathcal{R}$ is given by (7)), a reflection coefficient of $\alpha = 0.1$ and no source term ($\phi^{data,L} = \phi^{data,R} = 0$). In particular, the signature of $\mathbf{Q}$ is $(1, 2)$. In this case, results are satisfactory : the density, macroscopic velocity and temperature given by the resolution of the linearized Euler system are very close from those given by the linearized Boltzmann equation.

In the second example on Figure 2 we consider the equilibrium state given by

$$(\rho_*, u_*, \theta_*) = (1, 0, 1),$$

with diffuse reflection at boundaries (operator $\mathcal{R}$ is given by (7)), a reflection coefficient of $\alpha = 0.8$ and no source term ($\phi^{data,L} = \phi^{data,R} = 0$). This is a degenerate case : the signature of $\mathbf{Q}$ is here $(1, 1)$. Thus as noticed in the previous section, we have four conservation relations and two components to be find in order to define m_+^n.

Finally in the last example on figure 3 we present the case of no reflection at boundaries with no source term ($\phi^{data,L} = \phi^{data,R} = 0$). We choose the signature $(3, 0)$ for $\mathbf{Q}$. Again in this case the approximation obtained using the Euler system is really close to the results given by the Boltzmann equation.
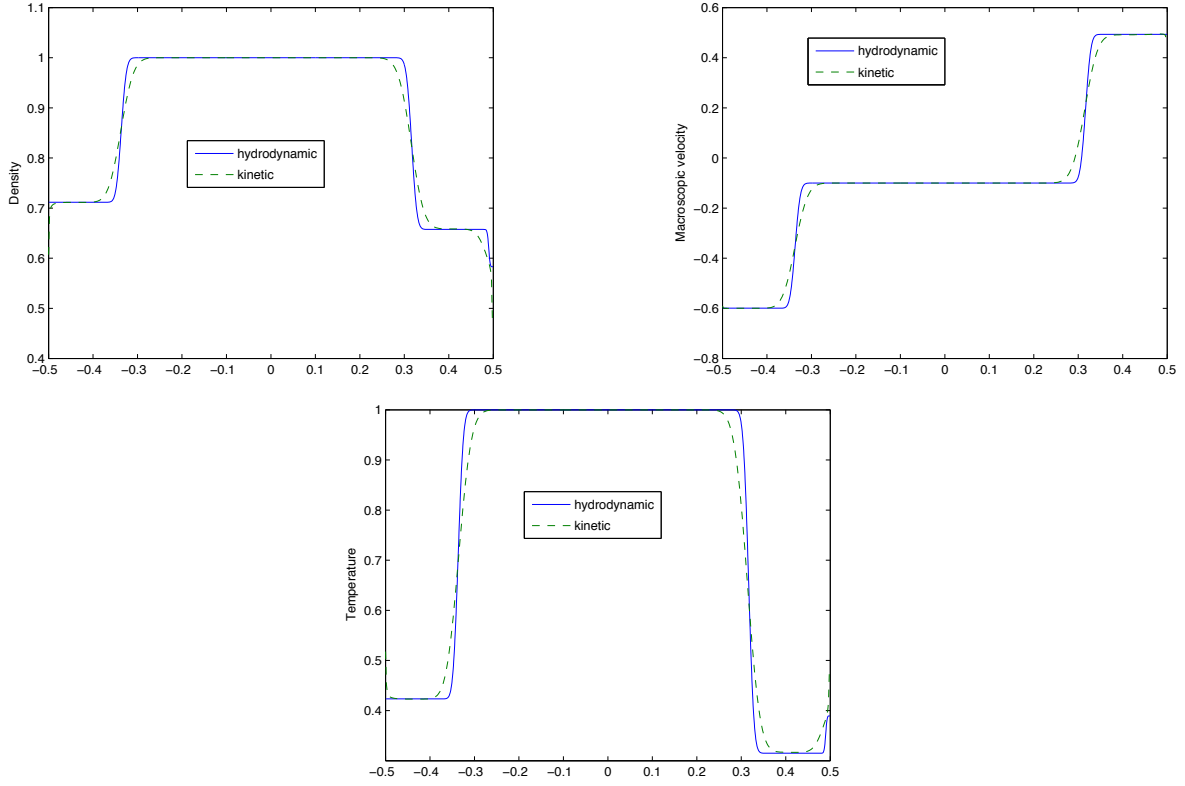
FIGURE 1. Comparison between the kinetic simulation and the hydrodynamic simulation at $t_f = 0.1$ s, for $(\rho_*, u_*, \theta_*) = (1, -0.1, 1)$, specular reflection at boundaries and $\alpha = 0.1$.

3. COUPLING WITH THE POISSON EQUATION

3.1. Analysis of the linearized Vlasov–Poisson system

In this section, we consider the linearization of the coupled Boltzmann–Poisson system (1)–(3). Let us assume that $\rho_* > 0$ and $\theta_* > 0$ are given. We set

$$\mathcal{M}_*(x,v) = \frac{\rho_* e^{-\frac{v^2}{2\theta_*}}}{\sqrt{2\pi\theta_*}} \frac{e^{-qV_*(x)/\theta_*}}{\int_{-\omega}^{\omega} e^{-qV_*(y)/\theta_*} \, dy} = M_{(\rho_*,0,\theta_*)}(v) \frac{e^{-qV_*(x)/\theta_*}}{\int_{-\omega}^{\omega} e^{-qV_*(y)/\theta_*} \, dy}. \tag{30}$$

We verify easily that for such a Maxwellian, we have

$$v\partial_x \mathcal{M}_* - q\partial_x V_* \partial_v \mathcal{M}_* = 0. \tag{31}$$

We choose for V_* the solution of the problem

$$\begin{cases} -\partial_{xx} V_* = q\left(\rho_* \dfrac{e^{-qV_*(x)/\theta_*}}{\int_{-\omega}^{\omega} e^{-qV_*(y)/\theta_*} \, dy} - 1\right), \\ V_*(-\omega) = V^L, \quad V_*(\omega) = V^R. \end{cases} \tag{32}$$

Lemma 1. *Assume V^L and V^R are given in $\mathbb{R}$ and $\rho_* > 0$, $\theta_* > 0$. Then there exists a unique solution $V_* \in C^2(-\omega, \omega)$ of the problem (32).*
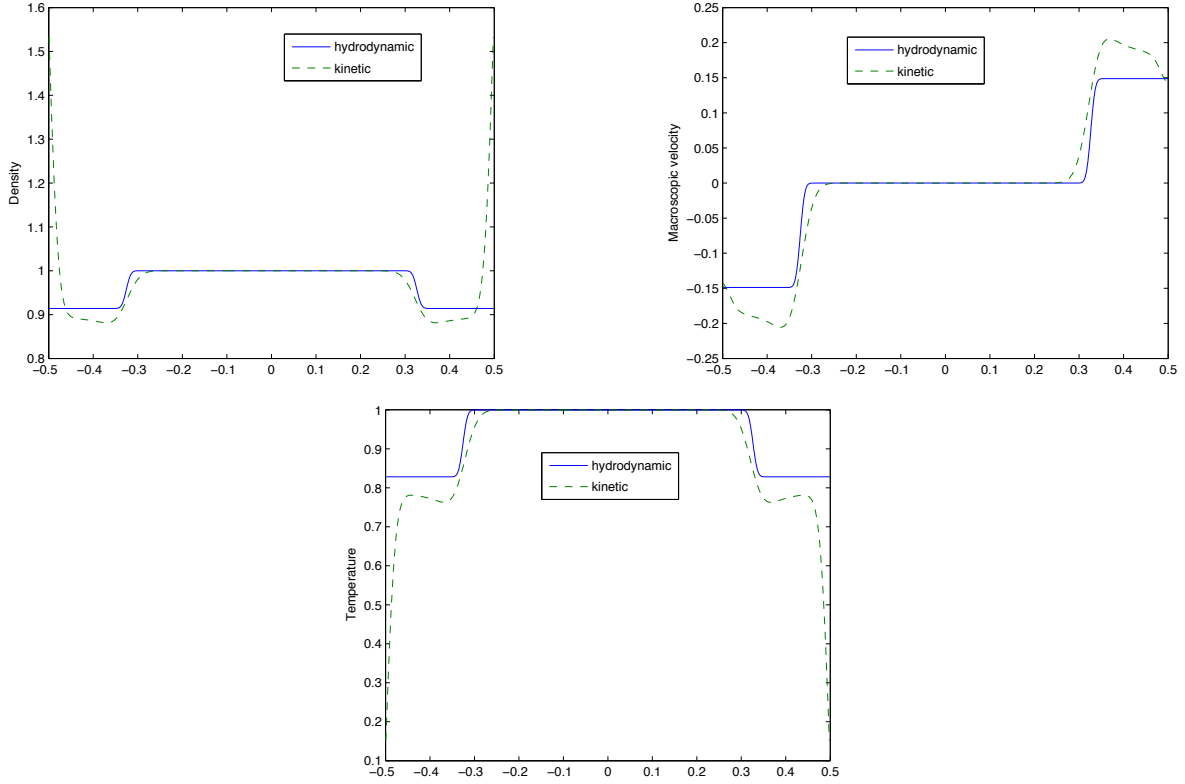
FIGURE 2. Comparison between the kinetic simulation and the hydrodynamic simulation at $t_f = 0.1$ s, for $(\rho_*, u_*, \theta_*) = (1, 0, 1)$, diffuse reflection at boundaries and $\alpha = 0.8$.

Proof. Let us define $V_b \in C^2([-\omega, \omega])$ an extension of the boundary condition: $V_b(-\omega) = V^L$ and $V_b(\omega) = V^R$. This results relies on the remark that a weak solution of (32) is a critical point in the affine space $V_b + H_0^1(-\omega, \omega)$ of the functional

$$J(V) = \frac{1}{2} \int_{-\omega}^{\omega} |\partial_x V|^2 \, dx - \rho_* \theta_* \ln \left(\int_{-\omega}^{\omega} e^{-qV/\theta_*} \, dx \right) - \int_{-\omega}^{\omega} qV \, dx.$$

Therefore, it remains to prove that this functional admits a unique minimizer. In fact, J is clearly continuous and convex on $H^1(-\omega, \omega)$ and we have the inequality

$$\ln \left(\int_{-\omega}^{\omega} e^{-qV/\theta_*} \, dx \right) \leq \frac{\|V\|_\infty}{\theta_*} + \ln(2\omega) \leq C\|V\|_{H^1} + \ln(2\omega).$$

Hence, applying the Poincaré inequality, we get

$$J(V) \geq \|V\|_{H^1}^2 - C_0 \rho_* \|V\|_{H^1} - C_1.$$

Then J is coercive and bounded from below on $H^1(-\omega, \omega)$. It admits a unique minimizer V_*. Applying standard techniques, we can show that $V_* \in C^2(-\omega, \omega)$. $\qquad\qquad\square$

Thus, the pair $(\mathcal{M}_*, V_*)$ is a stationary solution of the Boltzmann-Poisson problem (1)–(3). We linearize around this solution by setting $F = \mathcal{M}_* + \mathcal{M}_* f$ and $V = V_* + \widetilde{V}$ where f and $\widetilde{V}$ are assumed to be small perturbations. Keeping only the first order term, we are led to the following linearized Boltzmann-Poisson
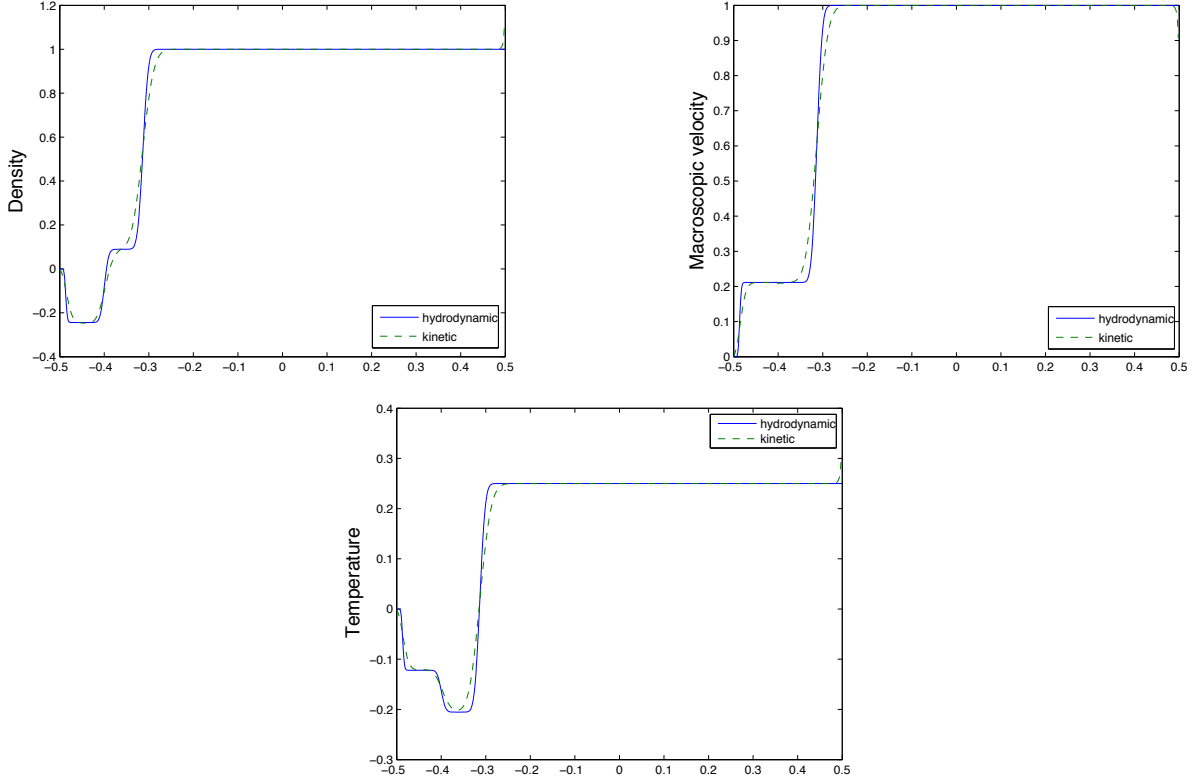
FIGURE 3. Comparison between the kinetic simulation and the hydrodynamic simulation at $t_f = 0.1$ s, for $(\rho_*, u_*, \theta_*) = (1, 1, 0.25)$, with no reflection and no source term at boundaries.

problem:

$$\partial_t f + v \partial_x f - q \partial_x V_* \partial_v f + q \frac{v}{\theta_*} \partial_x \widetilde{V} = \frac{1}{\tau} L_* f. \tag{33}$$

The linearized collision operator L_* has been defined in the previous section. Equation (33) is coupled to the Poisson equation

$$-\partial_{xx} \widetilde{V} = q \int_{\mathbb{R}} f \mathcal{M}_* \, dv, \qquad \widetilde{V}(-\omega) = \widetilde{V}(\omega) = 0. \tag{34}$$

Thus, as τ goes to 0 the function f looks like an infinitesimal Maxwellian $m_{(\widetilde{\rho}, \widetilde{u}, \widetilde{\theta})}$. The properties of L_* described above yield

$$\int_{\mathbb{R}} L_* f \begin{pmatrix} 1 \\ v \\ |v|^2 \end{pmatrix} M_{(\rho_*, 0, \theta_*)} \, dv = 0.$$

Therefore taking the moments of (33), we are led to the following system:

$$\partial_t \int_{\mathbb{R}} \begin{pmatrix} 1 \\ v \\ |v|^2 \end{pmatrix} f M_{(\rho_*, 0, \theta_*)} \, dv + \partial_x \int_{\mathbb{R}} v \begin{pmatrix} 1 \\ v \\ |v|^2 \end{pmatrix} f M_{(\rho_*, 0, \theta_*)} \, dv - q \partial_x V_* \int_{\mathbb{R}} \begin{pmatrix} 1 \\ v \\ |v|^2 \end{pmatrix} \partial_v f M_{(\rho_*, 0, \theta_*)} \, dv$$

$$+ q \frac{\partial_x \widetilde{V}}{\theta_*} \int_{\mathbb{R}} v \begin{pmatrix} 1 \\ v \\ |v|^2 \end{pmatrix} M_{(\rho_*, 0, \theta_*)} \, dv = 0.$$

11

Integrating by parts, we deduce

$$\int_{\mathbb{R}} \begin{pmatrix} 1 \\ v \\ |v|^2 \end{pmatrix} \partial_v f M_{(\rho_*,0,\theta_*)} \, dv = \int_{\mathbb{R}} \frac{v}{\theta_*} \begin{pmatrix} 1 \\ v \\ |v|^2 \end{pmatrix} f M_{(\rho_*,0,\theta_*)} \, dv - \int_{\mathbb{R}} \begin{pmatrix} 0 \\ 1 \\ 2v \end{pmatrix} f M_{(\rho_*,0,\theta_*)} \, dv$$

Substituting f by $m_{(\widetilde{\rho},\widetilde{u},\widetilde{\theta})}$, we use the identities

$$\int_{\mathbb{R}} m_{(\widetilde{\rho},\widetilde{u},\widetilde{\theta})} M_{(\rho_*,0,\theta_*)} \, dv = \widetilde{\rho}, \qquad \qquad \int_{\mathbb{R}} v m_{(\widetilde{\rho},\widetilde{u},\widetilde{\theta})} M_{(\rho_*,0,\theta_*)} \, dv = \rho_* \widetilde{u};$$

$$\int_{\mathbb{R}} v^2 m_{(\widetilde{\rho},\widetilde{u},\widetilde{\theta})} M_{(\rho_*,0,\theta_*)} \, dv = \rho_* \widetilde{\theta} + \widetilde{\rho}\theta_*, \qquad \qquad \int_{\mathbb{R}} v^3 m_{(\widetilde{\rho},\widetilde{u},\widetilde{\theta})} M_{(\rho_*,0,\theta_*)} \, dv = 3\rho_* \theta_* \widetilde{u}.$$

We deduce that

$$\partial_t \begin{pmatrix} \widetilde{\rho} \\ \widetilde{u} \\ \widetilde{\theta} \end{pmatrix} + \begin{pmatrix} 0 & \rho_* & 0 \\ \frac{\theta_*}{\rho_*} & 0 & 1 \\ 0 & 2\theta_* & 0 \end{pmatrix} \partial_x \begin{pmatrix} \widetilde{\rho} \\ \widetilde{u} \\ \widetilde{\theta} \end{pmatrix} = q \partial_x V_* \begin{pmatrix} \frac{\rho_* \widetilde{u}}{\theta_*} \\ \frac{\widetilde{\theta}}{\theta_*} \\ 0 \end{pmatrix} - q \partial_x \widetilde{V} \begin{pmatrix} 0 \\ 1 \\ 0 \end{pmatrix} \qquad (35)$$

holds. From (34), this system is coupled with the linearized Poisson equation

$$-\partial_{xx} \widetilde{V} = q \, \widetilde{\rho} \frac{e^{-qV_*(x)/\theta_*}}{\int_{-\omega}^{\omega} e^{-qV_*(y)/\theta_*} \, dy}, \qquad \widetilde{V}(-\omega) = \widetilde{V}(\omega) = 0. \qquad (36)$$

Like for the free problem, we assume that f admits an expansion of the form

$$f = m_{(\widetilde{\rho},\widetilde{u},\widetilde{\theta})} + G^L(t, \frac{x+\omega}{\tau}, v) + G^R(t, \frac{\omega-x}{\tau}, v) + \mathrm{o}(\tau).$$

Then the boundary layers G^L and G^R satisfies the same half space problem (17). Therefore the determination of the boundary condition that we have to impose to solve (35) follows the treatment presented in the previous section. We notice moreover that we are necessary in the degenerate case where the quadratic form associated to the matrix of the hyperbolic equation has the signature $(1,1)$, i.e. $u_* = 0$. In fact, if we choose non-zero u_*, the relation (31) is not satisfied and therefore $\mathcal{M}_*$ is not a stationary solution of the Boltzmann equation.

We present some comparisons between the simulation of the linearized Boltzmann-Poisson equation and the linearized Euler-Poisson system. In the numerical procedures we use, system (32) is solved thanks to a fixed point iterative procedure. Since ρ_* and θ_* are fixed, the potential V_* is computed only once for all at the beginning of the simulation. The linearized Boltzmann equation (33) is solved with the same idea than in the previous section : we split by solving first the transport equation on one time step

$$\partial_t f + v\partial_x f - q\partial_x V_* \partial_v f + q\frac{v}{\theta_*}\partial_x \widetilde{V} = 0,$$

with an upwind scheme, then we solve on one time step

$$\partial_t f = \frac{1}{\tau} L_*(f).$$

The linearized Euler system (35) is discretized by a splitting method: first we solve (35) with zero at the right hand side as described in subsection 2.2.1 and then we solve implicitly

$$\partial_t \begin{pmatrix} \widetilde{\rho} \\ \widetilde{u} \\ \widetilde{\theta} \end{pmatrix} = q\partial_x V_* \begin{pmatrix} \frac{\rho_* \widetilde{u}}{\theta_*} \\ \frac{\widetilde{\theta}}{\theta_*} \\ 0 \end{pmatrix} - q\partial_x \widetilde{V} \begin{pmatrix} 0 \\ 1 \\ 0 \end{pmatrix}.$$

The Poisson equation is discretized thanks to a finite difference method. Figures 4 and 5 present the results for a linearization around the equilibrium state given by $(\rho_*, u_*, \theta_*) = (1, 0, 0.5)$, with a source term at the boundaries in Figure 4 and in the case of specular reflection in Figure 5.
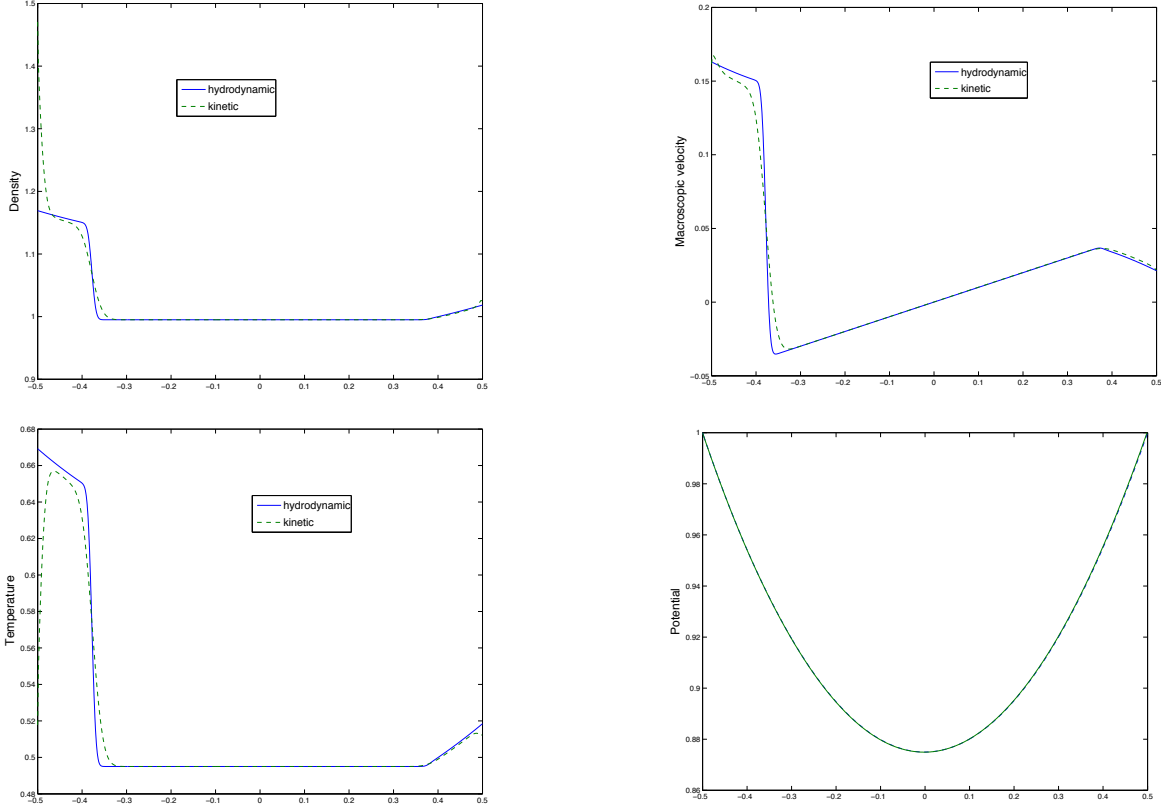
FIGURE 4. Comparison between the kinetic simulation and the hydrodynamic simulation for the coupled problem with $(\rho_*, u_*, \theta_*) = (1, 0, 0.5)$, no reflection at boundaries ($\mathcal{R} = 0$), $\phi^{data,L} = m_{(2/1.2,0,1.2/2)}$, $\phi^{data,R} = m_{(\rho_*,0,\theta_*)}$, $q = -1$, $V^L = V^R = 1$ at $t_f = 0.1$.

3.2. The non-linear Euler–Poisson system

Finally, we come back to the non-linear problem (1)–(3) presented in the introduction. As the mean free path goes to 0, we get the Euler-Poisson system:

$$\begin{cases} \partial_t \rho + \partial_x(\rho u) = 0, \\[2mm] \partial_t(\rho u) + \partial_x(\rho u^2 + \rho\theta) = -q\rho\partial_x V, \\[2mm] \partial_t\left(\frac{\rho\theta + \rho u^2}{2}\right) + \partial_x\left(\frac{3}{2}\rho u\theta + \frac{1}{2}\rho u^3\right) = -q\rho u\partial_x V, \end{cases} \tag{37}$$

coupled to

$$-\partial_{xx}V = q(\rho - 1). \tag{38}$$

We present a first attempt to treat numerically the initial-boundary-value problem, incorporating the computation of relevant boundary conditions for the hydrodynamics, designed following the approach used for the neutral problem and the linearized equation. Clearly nonlinearities and coupling give rise to new difficulties and this work has to be considered as a preliminary step towards the simulation of physically relevant cases.
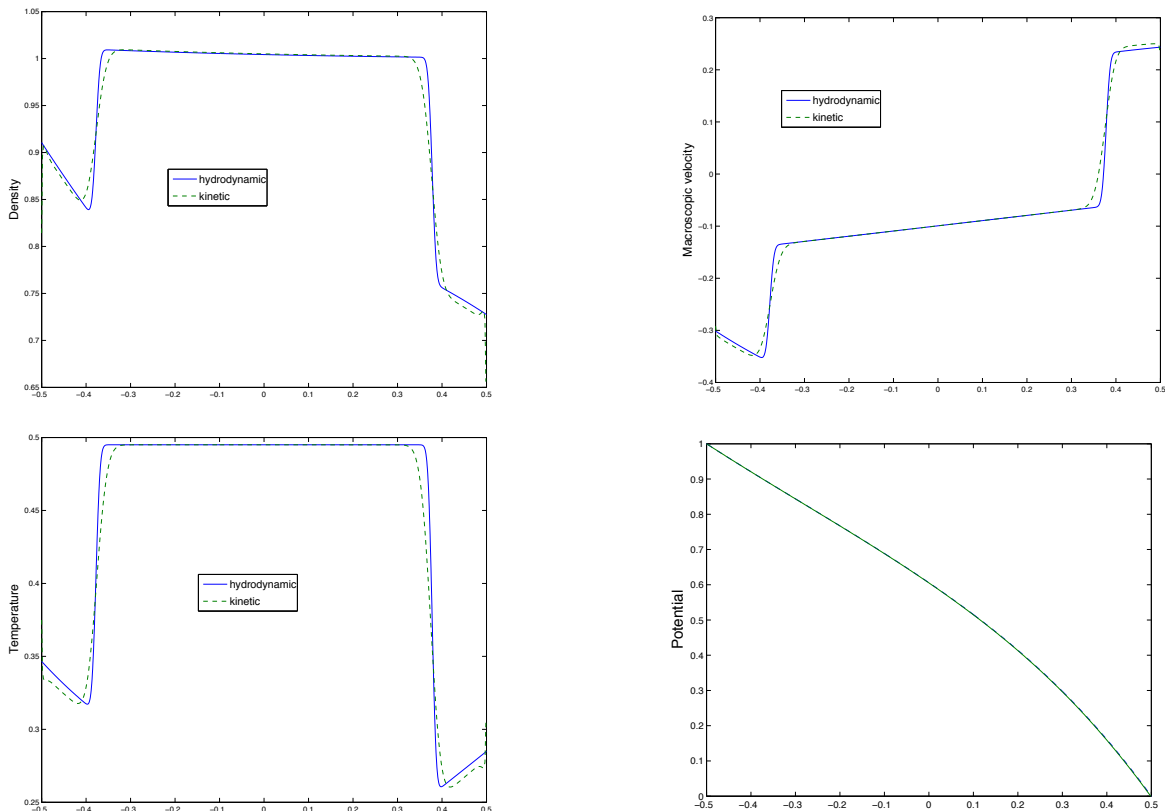
13

FIGURE 5. Comparison between the kinetic simulation and the hydrodynamic simulation for the Poisson problem with $(\rho_*, u_*, \theta_*) = (1, 0, 0.5)$, specular reflection at boundaries with $\alpha = 0.4$, $\phi^{data,L} = \phi^{data,R} = 0$, $q = 1$, $V^L = 1$, $V^R = 0$ at $t_f = 0.1$.

Here the hydrodynamic problem is not linear and we will use a finite volume scheme to discretize (37). As above, we fix a regular subdivision $\{x_0, \ldots, x_{I+1}\}$ of the domain $[-\omega, \omega]$, with $x_i = -\omega + i\Delta x$ and $\Delta x = 2\omega/(I+1)$, and denote $C_i = (-\omega + (i-1/2)\Delta x, -\omega + (i+1/2)\Delta x)$ the cell centered in x_i for $i = 1, \ldots, I$. Let us denote $\mathcal{U}$ the vector $(\rho, \rho u, \frac{1}{2}(\rho\theta + \rho u^2))$. Then $\mathcal{U}_i^n$ is an approximation of $\frac{1}{\Delta x} \int_{C_i} \mathcal{U}(n\Delta t, x)\, dx$; it is computed thanks to a discretization of (37) (see e.g. [4, 11, 16, 21]):

$$\mathcal{U}_i^{n+1} - \mathcal{U}_i^n = -\frac{\Delta t}{\Delta x}(\mathcal{F}_{i+1/2}^n - \mathcal{F}_{i-1/2}^n),$$

where $\mathcal{F}_{i+1/2}^n$ is an approximation of the flux at the interface between C_i and C_{i+1}. In this work, we use the Godounov fluxes to approximate this quantity (see e.g. [11, 12]); it is then determined by the computed quantities in the two neighboring cells : $\mathcal{F}_{i+1/2}^n = F(\mathcal{U}_i^n, \mathcal{U}_{i+1}^n)$. Therefore the macroscopic quantities at time $(n+1)\Delta t$ are entirely determined, provided we compute the fluxes at the boundary of the domain. The idea to raise this question is to linearize around a steady state. Then we get the linearized problem presented in the previous subsection and can compute as previously the boundary conditions. The Poisson equation (38) is then discretized thanks to the finite difference method.

The first difficulty is to determine a steady state around which we linearize. As already noticed in [2], we need to update this state at each time step and to linearize locally. More precisely, let us assume that the state $\mathcal{U}^n$ at time $t^n = n\Delta t$ is known. Therefore, we know an approximation of ρ and θ in the cells C_1 and C_I at time t^n. We will use these values to linearize the Boltzmann-Poisson system. Let us detail for instance the treatment of the left boundary $x = -\omega$. We take ρ_* and θ_* to be respectively equal to the computed

14

values of ρ and θ in the cells C_1 at time t^n. Then, solving system (32), we deduce V_* and linearize then around the state $\mathcal{M}_*$ defined thanks to ρ_*, θ_* and V_*. We have therefore $F = \mathcal{M}_*(1 + m_{(\widetilde{\rho},\widetilde{u},\widetilde{\theta})} + G^L + o(\tau))$. The fluxes are given by

$$\begin{pmatrix} \rho u \\ \rho u^2 + \rho\theta \\ (\rho u^2 + 3\rho\theta)u \end{pmatrix} = \int_{\mathbb{R}} v \begin{pmatrix} 1 \\ v \\ |v|^2 \end{pmatrix} F(v)\, dv = \int_{\mathbb{R}} v \begin{pmatrix} 1 \\ v \\ |v|^2 \end{pmatrix} \mathcal{M}_*(v)(1 + m_{(\widetilde{\rho},\widetilde{u},\widetilde{\theta})})\, dv,$$

where we use the conservation identity

$$\int_{\mathbb{R}} v \begin{pmatrix} 1 \\ v \\ |v|^2 \end{pmatrix} G^L(z,v) M_*(v)\, dv = 0,$$

for all $z \geq 0$. It follows that

$$\begin{pmatrix} \rho u \\ \rho u^2 + \rho\theta \\ (\rho u^2 + 3\rho\theta)u \end{pmatrix} = \frac{e^{-qV_*(x)/\theta_*}}{\int_{-\omega}^{\omega} e^{-qV_*(y)/\theta_*}\, dy} \begin{pmatrix} \rho_*\widetilde{u} \\ \rho_*\theta_* + \widetilde{\rho}\theta_* + \rho_*\widetilde{\theta} \\ 3\rho_*\theta_*\widetilde{u} \end{pmatrix}.$$

Thus we deduce the boundary fluxes provided we know the boundary values of the linearized quantities $(\widetilde{\rho},\widetilde{u},\widetilde{\theta})$. These values are computed using the method described in the previous subsection for the linearized Boltzmann-Poisson system.

Numerical results are presented in Figures 6, 7 and 8 in the case of a population of electrons (i.e. $q = -1$). In Figures 6 and 7 we choose an initial value such that $(\rho, u, \theta) = (0.5, 0, 1)$ therefore we take $F^{init} = M_{(0.5,0,0,1)}$ in the kinetic model. In Figure 8 the initial data is chosen such that $(\rho, u, \theta) = (1, 0, 1)$. Figure 6 displays the result obtained in the case of specular reflection with $\alpha = 0.5$. In Figures 7 and 8 we present the case of a source term at the boundaries. In figure 7 we consider $\Phi^{data,L} = M_{(1.2,0,1.2/2)}$, $\Phi^{data,R} = M_{(1,0,0.5)}$, and in figure 8 $\Phi^{data,L} = M_{(1.2/1.1,0,1.1/2)}$, $\Phi^{data,R} = M_{(1,0,1)}$.

CONCLUSIONS AND PERSPECTIVES

In this work, according to [2] we present a numerical method for defining the boundary conditions of the linearized Euler system accounting from the formation of Knudsen boundary layers. The boundary conditions are based on the Maxwell approximation of the fluxes of the underlying kinetic half–space problem. This approach is extended to treat the Euler–Poisson system both in the linearized and non–linear versions. We detail how we can bypass the difficulties induced by the coupling with the electric field.

However, this work is a preliminary attempt and the schemes can be improved in several ways. First of all, the splitting scheme we are using for solving the Euler–Poisson system is not very elaborate, especially for the the non–linear model which would deserve a deeper analysis. Furthermore, with this scheme steady states solutions are not preserved numerically. Definitely, the design of a specific Well–Balanced scheme looks appropriate for this problem, see [5]. Second of all, the Maxwell approximation is simple but certainly too rough. Improving the evaluation of the asymptotic state and outgoing distribution of the half–space problem is a crucial issue to reduce the discrepancies observed between the hydrodynamic and kinetic simulations. A possible path for this purpose can be inspired by the approximations designed in [14]. Finally, for most applications in plasma physics the interactions between electrons and positive charges have a crucial role. It implies to deal with coupled systems of kinetic or hydrodynamic equations, instead of describing a single specie. Moreover, boundary conditions for the potential are also driven by intricate charge phenomena, which involve the fluxes of charged particles. Details on the modeling issues in the context of spacecraft engineering can be found in [6–8, 17, 20, 23]. Depending on the physical characteristics of the plasma, it can be relevant to use hydrodynamic systems instead of kinetic models, see [3]. At least, reducing the variables dimension and getting rid of stiff terms allow a substantial gain in terms of computational cost. However it left open the question of the boundary conditions to be used for the hydrodynamic fluxes, which
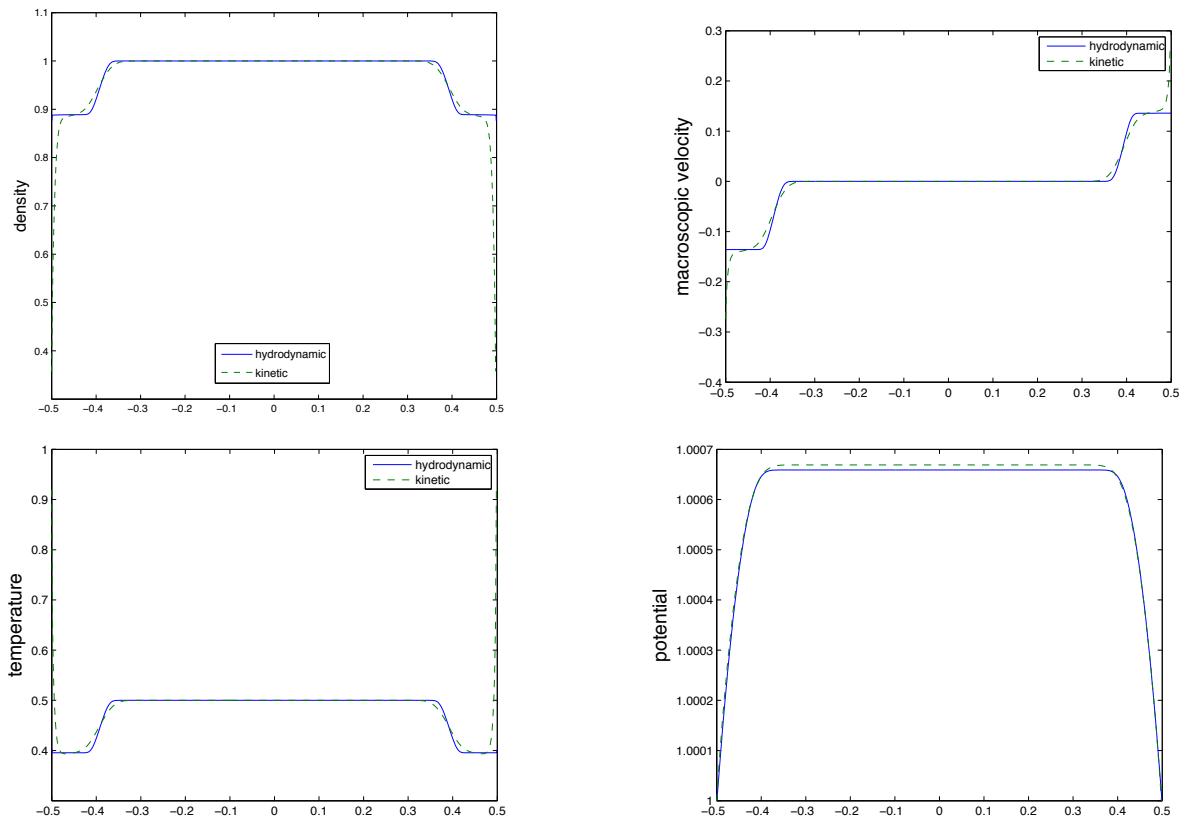
FIGURE 6. Comparison between the kinetic simulation and the hydrodynamic simulation for the Poisson problem with specular reflection at boundaries with $\alpha = 0.5$ and no source term, $q = -1$, $V^L = V^R = 1$ at final time $t_f = 0.1$.

motivates the present work. It is likely however, for such applications, that the main difficulty is related to the treatment of the boundary conditions for the potential. This question is beyond the scope of this paper and we expect the numerical strategy we have introduced will be a useful contribution towards the simulation of these phenomena.

References

[1] A. Arnold and U. Giering, *An analysis of the Marshak conditions for matching Boltzmann and Euler equations*, Math. Models Methods Appl. Sci., 7(4), 557–577, 1997.

[2] C. Besse, S. Borghol, T. Goudon, I. Lacroix-Violet, J.-P. Dudon, *Hydrodynamic regimes, Knudsen layer, numerical schemes: definition of boundary fluxes*, to appear in Adv. Appl. Math. Mech.

[3] S. Borghol, *Modélisation mathématique de la charge de surface des satellites en orbite basse*, PhD Thesis, Université Lille 1, 2010.

[4] F. Bouchut, *Nonlinear stability of finite volume methods for hyperbolic conservation laws and well-balanced schemes for sources*, Frontiers in Mathematics. Birkhauser Verlag, Basel, 2004.

[5] F. Bouchut, T. Morales, *A subsonic-well-balanced reconstruction scheme for shallow water flows*, SIAM J. Numer. Anal., 48, 1733–1758, 2010.

[6] O. Chanrion, *Simulation de l'influence de la propulsion plasmique sur la charge électrostatique dÕun satellite en milieu magnétosphérique*, PhD Thesis, Ecole Nationale des Ponts et Chaussées, 2001.

[7] M. Chane-Yook, S. Clerc, S. Piperno, *Space charge and potential distribution around a spacecraft in a isotropic plasma*, J. Geophys. Res. - Space Physics 111, 2006.

[8] S. Clerc, S. Brosse, M. Chane-Yook, `Sparcs`: *an advanced software for spacecraft charging analysis*, 8th Spacecraft Charging Tech. Conf., Huntsville, Alabama, 2003.
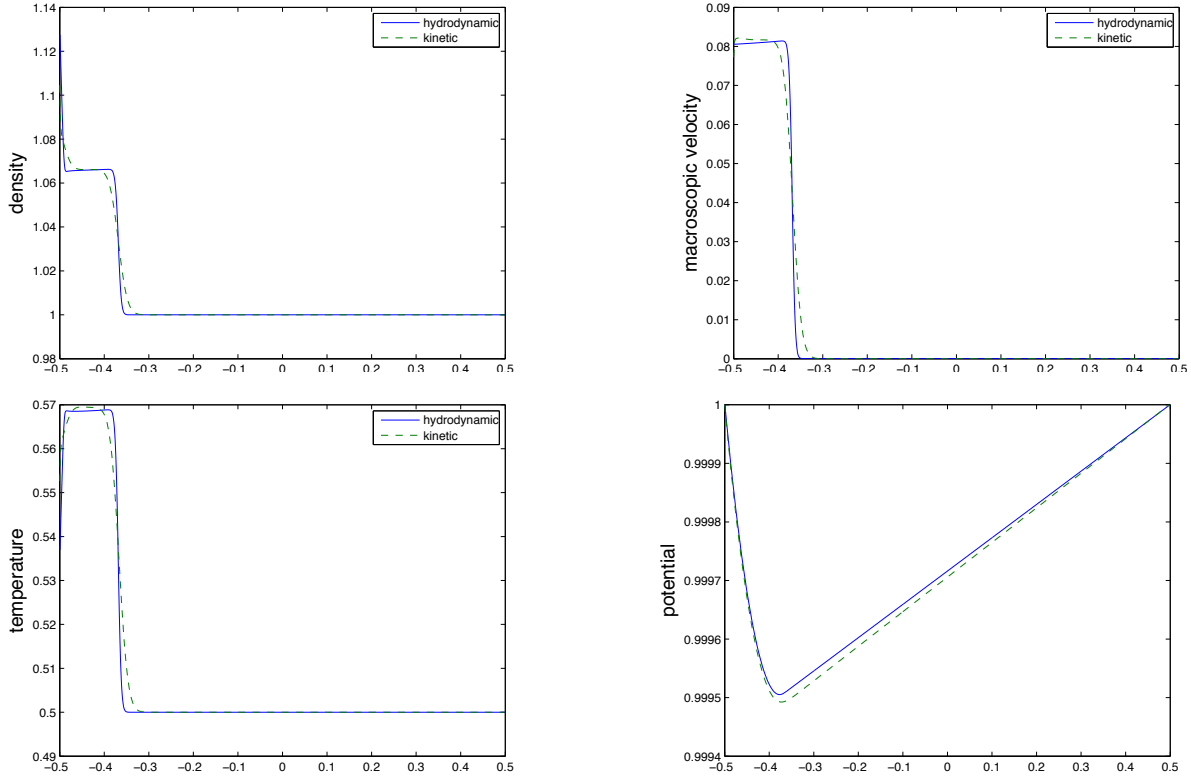
FIGURE 7. Comparison between the kinetic simulation and the hydrodynamic simulation for the Poisson problem with source term $\Phi^{data,L} = M_{(1.2,0,1.2/2)}$, $\Phi^{data,R} = M_{(1,0,0.5)}$ and no reflection, $q = -1$, $V^L = V^R = 1$ at $t_f = 0.1$.

[9] F. Coron, F. Golse, C. Sulem, *A classification of well-posed kinetic layer problems*, Comm. Pure Appl. Math., 41(4), 409–435, 1988.

[10] S. Dellacherie. *Coupling of the Wang Chang-Uhlenbeck equations with the multispecies Euler system*, J. Comput. Phys., 189, 239–276, 2003.

[11] E. Godlewski and P.-A. Raviart, *Numerical approximation of hyperbolic systems of conservation laws*, volume 118 of Applied Mathematical Sciences. Springer, New-York, 1996.

[12] S. K. Godounov, *Lois de conservation et intégrales d'énergie des équations hyperboliques* in C. Carasso, P.-A. Raviart, and D. Serre, editors, *Nonlinear hyperbolic problems* (St. Etienne, 1986), volume 1270 of Lecture Notes in Math., pp. 135–149. Springer, Berlin, 1987.

[13] F. Golse, *Boundary and interface layers for kinetic models*, Technical report, GdR SPARCH-CNRS, September 1997. Lecture Notes of the 4th Summer School of the GdR SPARCH, St Pierre d'Oléron.

[14] F. Golse, A. Klar, *A numerical method for computing asymptotic states and outgoing distributions for kinetic linear half-space problem*, J. Stat. Phys., 80(5/6), 1033–1061, 1995.

[15] T. Goudon, *Existence of solutions of transport equations with nonlinear boundary conditions*, European J. Mech. B Fluids, 16(4):557–574, 1997.

[16] R. J. LeVeque *Finite volume methods for hyperbolic problems*, Cambridge Texts in Applied Mathematics. Cambridge University Press, Cambridge, 2002.

[17] L. Lévy, *Charge des matériaux et systèmes en environnement spatial*, CERT–ONERA, in *Space environment prevention of risks related to spacecraft charging*, Editions Cepaduès, Toulouse, France, 1996.

[18] R. E. Marshak, *Note on the spherical harmonic method as applied to the Milne problem for a sphere*, Phys. Rev., 71, 443–446, 1947.

[19] J. C. Maxwell, *On stresses in rarified gases arising from inequalities of temperature*, Phil. Trans. Royal Soc. London, 170, 231–256, 1879.

[20] J.-F. Roussel, *Modelling of spacecraft plasma environment interactions*, in *Spacecraft Charging Technology*, Proceedings of the Seventh International Conference held 23Ð27 April, 2001 at ESTEC, Noordwijk, The Netherlands, R.A. Harris Ed., European Space Agency, ESA SP-476, 2001.
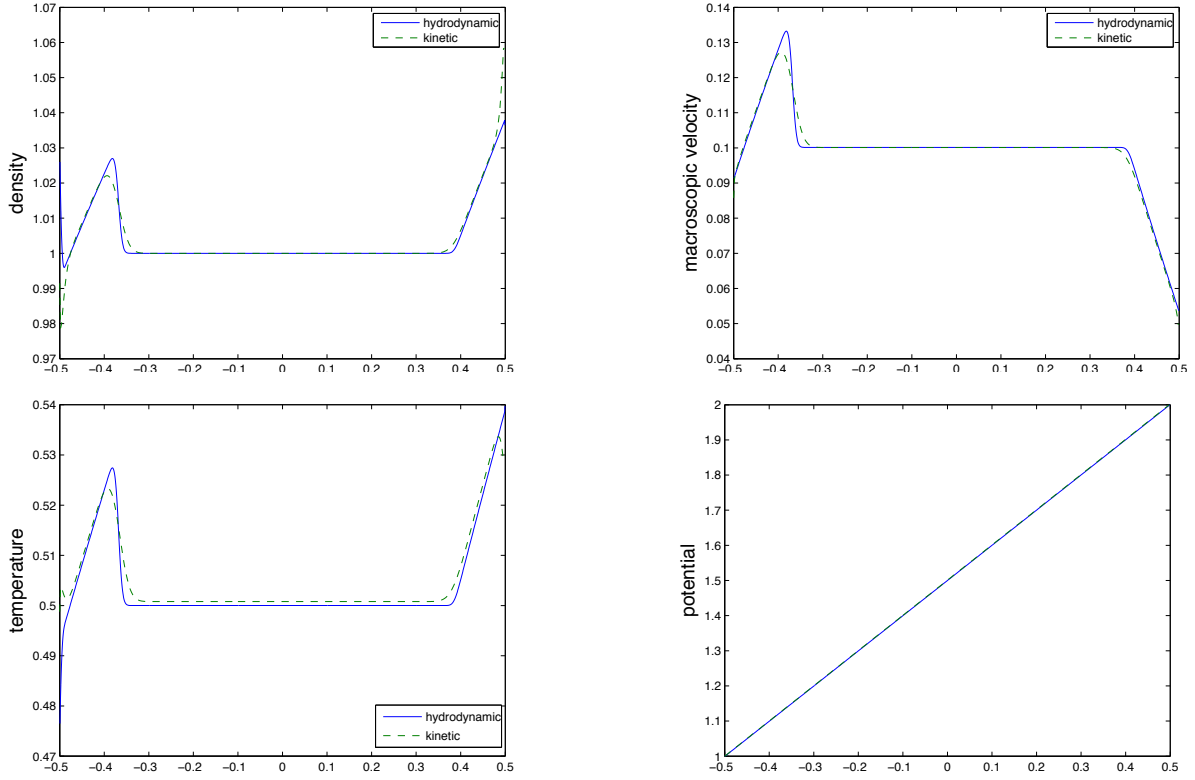
FIGURE 8. Comparison between the kinetic simulation and the hydrodynamic simulation for the Poisson problem with source term $\Phi^{data,L} = M_{(1.2/1.1,0,1.1/2)}$, $\Phi^{data,R} = M_{(1,0,0.5)}$ and no reflection, $q = -1$, $V^L = 1$ and $V^R = 2$ at $t_f = 0.1$.

[21] D. Serre, *Systems of conservation laws, Volume 1: Hyperbolicity, entropies, shock waves*, Cambridge University Press, Cambridge, 1999.

[22] A. Vasseur, *Rigorous derivation of the kinetic/fluid coupling involving a kinetic layer on a toy problem*, to appear in Archiv. Rat. Mech. Anal.

[23] N. Vauchelet, C. Besse, J.-P. Dudon, T. Goudon, *Comparison of Vlasov solvers for spacecraft charging simulation*, Math. Modelling and Numerical Analysis (M2AN), 44, 109–131, 2010.